Electronic Supplementary Information

Synthesis and Photophysical Properties of a New Push–Pull Pyrene Dye with Green-to-Far-red Emission and its Application to Human Cellular and Skin Tissue Imaging

Kazuki Inoue,[†a] Ryosuke Kawakami,[†b] Masamoto Murakami,[c] Taku Nakayama,[d] Shinkuro Yamamoto,[d] Keiji Inoue,[d] Teruko Tsuda,[c] Koji Sayama,[c] Takeshi Imamura,[b] Daisuke Kaneno,[e] Shingo Hadano,[a] Shigeru Watanabe[a] and Yosuke Niko*[a]

[a]Research and Education Faculty, Multidisciplinary Science Cluster, Interdisciplinary Science Unit, Kochi University, 2-5-1 Akebono-cho, Kochi-shi, Kochi 780-8520, Japan.

[b]Department of Molecular Medicine for Pathogenesism, Graduate School of Medicine, Ehime University, Shitsukawa, Toon, Ehime 791-0295, Japan.

[c]Department of Dermatology, Graduate School of Medicine, Ehime University, Shitsukawa, Toon, Ehime 791-0295, Japan.

[d]Center for Photodynamic Medicine Kochi Medical School, Kochi University, Kohasu, Oko-cho, Nankoku, Kochi 783-8505, Japan.

[e]Department of Applied Science, Graduate School of Integrated Arts and Sciences, Kochi University, 200 Otsu, Monobe, Nankoku City, Kochi 783-8502, Japan.

* Corresponding author. E-mail: y.niko@kochi-u.ac.jp

† These authors contributed equally to this work.

Table of Contents

1. Synthetic procedures of **PC** and **PC2**
2. Absorption spectra of **PC** and **PK** in solvents of different polarities
3. Determination of the change in the dipole moment between the ground and excited states of **PC** and **PK** using the Lippert–Mataga and Bakhshiev equations
4. Optimized structures and dipole moments of **PC** and **PK** in the ground and excited states
5. Time-resolved fluorescence decay of **PC** and **PK** in large unilamellar vesicles (LUVs) of different lipid compositions
6. Confocal laser scanning fluorescence microscopy (CLSM) images of PC3 cells stained by **PC** and Lipi-Deep Red.
7. Cytotoxicities of **PC** and **PK**
8. Comparison of **PC**, **PK**, and Nile Red (**NR**) in human tissue imaging using two-photon fluorescence microscopy (2PM)
9. ^{1}H and ^{13}C NMR spectra of **PC** and **PC2**
10. References

1. Synthetic procedures of PC and PC2

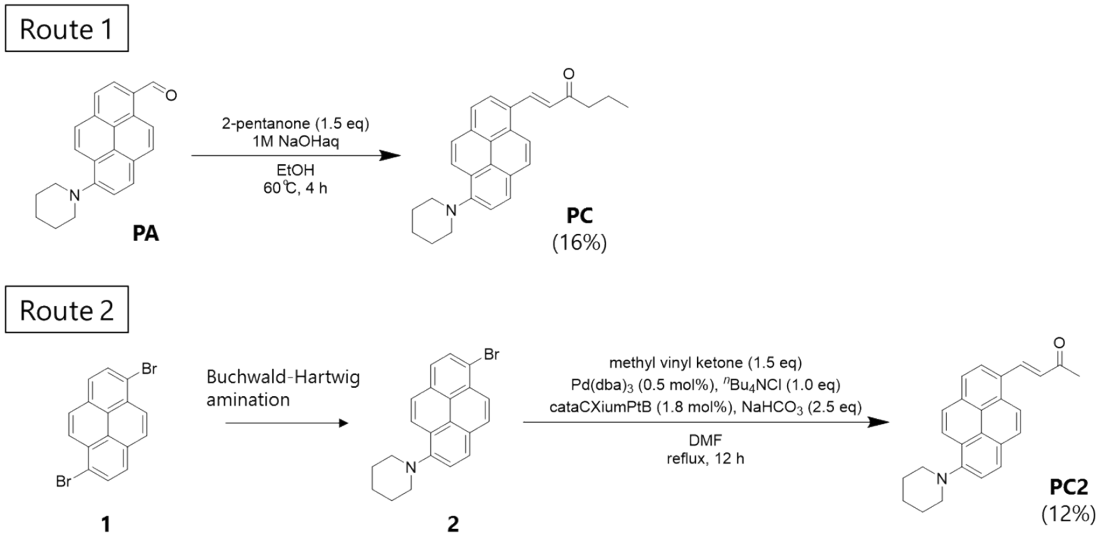

Scheme S1. Synthetic routes for the newly designed pyrene-based push–pull dye (**PC**) and its analog (**PC2**). The synthetic procedures for **PA** and **2** are described in another study.[1] Definitions: dba = dibenzylideneacetone; DMF = *N*,*N*-dimethylformamide.

*Synthesis of **PC** (Route 1)*

To a mixture of **PA** (100 mg, 0.32 mmol) and 2-pentanone (47 μL, 0.48 mmol) in ethanol (6 mL) was added 1 M NaOH (aq., 1 mL). The resulting mixture was stirred for 4 h at 60 °C under an argon atmosphere. Water was added to the mixture, and the resulting precipitate was filtered. The filtered crude compound was purified by column chromatography on silica gel (dichloromethane:hexane = 2:1) and subsequent recrystallization from acetonitrile to afford **PC** as an orange solid (20 mg, 16%). Mp: 150.4–151.7 °C, ^{1}H NMR (500 MHz, $CDCl_3$, TMS) δ: 8.71 (1H, d, J = 15.8), 8.45 (1H, d, J = 9.1), 8.32 (1H, d, J = 9.2), 8.25 (1H, d, J = 8.1), 8.14 (1H, d, J = 8.1), 8.08 (1H, d, J = 8.0), 8.08 (1H, d, J = 9.2), 8.03 (1H, d, J = 9.1), 7.74 (1H, d, J = 8.0), 7.01 (1H, d, J = 15.8), 3.21 (4H, br), 2.78 (2H, t, J = 7.3), 1.92–1.94 (4H, m), 1.77–1.84 (2H, m), 1.73 (2H, br), 1.05 (3H, t, J = 7.3). ^{13}C NMR (125 MHz, $CDCl_3$, TMS) δ 200.5, 150.3, 139.3, 133.2, 130.8, 128.7, 127.7, 127.6, 126.6, 126.5, 126.3, 126.0, 125.7, 125.1, 124.7, 124.5, 124.3, 120.5, 117.5, 55.2, 43.5, 26.8, 24.6, 18.1, 14.1. HRMS (ESI), *m/z*: [M] calcd for $C_{27}H_{27}NO$, 380.2020; found, 380.2049.

*Synthesis of **PC2** (Route 2)*

To a mixture of **2** (200 mg, 0.54 mmol), $Pd(dba)_3$ (3 mg, 0.003 mmol), cataCXium®PtB (3.2 mg, 0.01 mmol), $^{n}Bu_4NCl$ (150 mg, 0.54 mmol), and $NaHCO_3$ (113 mg, 1.35 mmol)

in dry DMF (3 mL) was added methyl vinyl ketone (66 µL, 0.81 mmol), and the resulting mixture was refluxed for 12 h under an argon atmosphere. After cooling to room temperature, the resulting precipitate was filtered and dichloromethane was added to the filtrate. The organic layer was washed with water and brine, dried over $MgSO_4$, and filtered. The solvent was evaporated *in vacuo*, and the residue was purified by silica gel column chromatography eluting with dichloromethane to obtain **PC2** as an orange solid (23 mg, 12%). Mp: 201.9–203.4 °C ^{1}H NMR (500 MHz, $CDCl_3$, TMS) δ: 8.67 (1H, d, *J* = 16.0), 8.46 (1H, d, *J* = 9.1), 8.31 (1H, d, *J* = 9.2), 8.25 (1H, d, *J* = 8.2), 8.15 (1H, d, *J* = 8.2), 8.09 (1H, d, *J* = 8.1), 8.09 (1H, d, *J* = 9.2), 8.03 (1H, d, *J* = 9.1), 7.75 (1H, d, *J* = 8.1), 7.00 (1H, d, *J* = 16.0), 3.21 (4H, br), 2.52 (3H, s), 1.91–1.94 (4H, m), 1.72 (2H, br). ^{13}C NMR (125 MHz, CDCl3, TMS) δ 198.3, 150.4, 140.3, 133.3, 130.7, 128.8, 128.4, 127.4, 126.6, 126.5, 126.3, 126.0, 125.7, 125.1, 124.8, 124.5, 124.3, 120.3, 117.5, 55.2, 28.1, 26.8, 24.6. HRMS (ESI), *m/z*: [M] calcd for $C_{25}H_{23}NO$, 353.1780; found, 353.1773.

2. Absorption spectra of PC and PK in solvents of different polarities

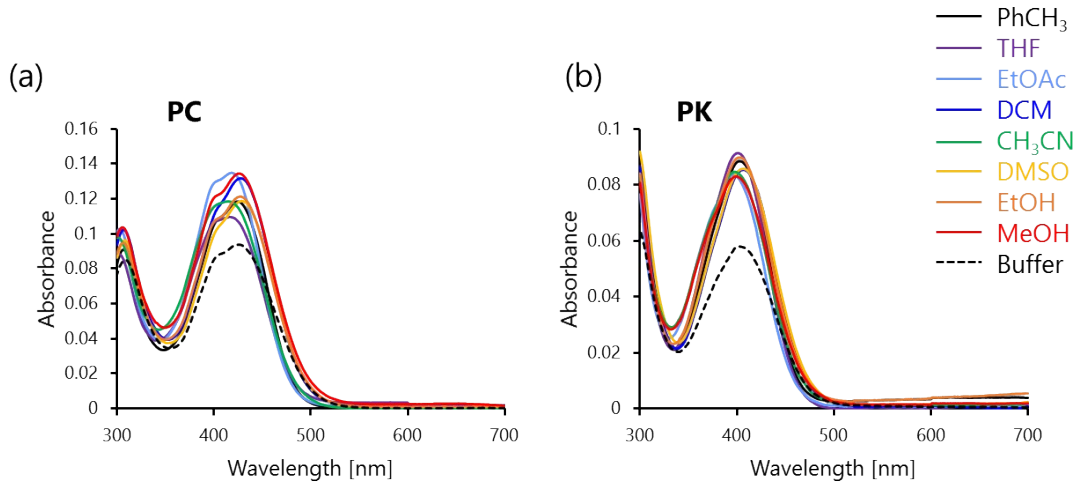

Figure S1. Absorption spectra of (a) **PC** and (b) **PK** in solvents of different polarities. Dye concentration: 5 μM.

3. Determination of the change in the dipole moment between the ground and excited states of PC and PK using the Lippert–Mataga and Bakhshiev equations

In the following equations, ν_a and ν_f denote the absorption and fluorescence maxima wavenumbers in cm^{-1} ($\nu_a - \nu_f$ means Stokes shift), respectively. ε and n are the dielectric constant and refractive index of the solvent, respectively. μ_e and μ_g denote the dipole moments of a dye in the excited and ground states ($\delta\mu = \mu_e - \mu_g$), respectively. h and c are Planck's constant and the velocity of light in a vacuum, respectively. a is the Onsager radius of the dye. Here, the a values of **PC** and **PK** were estimated from density functional theory (DFT) calculations using the Gaussian 09 program package.[2] Specifically, the equilibrium structures of **PC** and **PK** were fully optimized using the M062X method with the 6-31+G** basis set. The analytical frequencies were obtained to ensure that a local energy minimum was located. Then, the molecular volumes of the optimized structures were calculated by the Monte Carlo method using the DFT density based on the 0.001 electrons/Bohr^3 density envelope.

Lippert–Mataga equation:[3]

$$\nu_a - \nu_f = m_1 F_1(\varepsilon,n) + constant$$

$$F_1(\varepsilon,n) = \left[\frac{\varepsilon - 1}{2\varepsilon + 1} - \frac{n^2 - 1}{2n^2 + 1}\right]$$

$$m_1 = \frac{2}{hca^3}(\mu_e - \mu_g)^2$$

Bakhshiev's equation:[4]

$$\nu_a - \nu_f = m_2 F_2(\varepsilon,n) + constant$$

$$F_2(\varepsilon,n) = \frac{2n^2 + 1}{n^2 + 2}\left[\frac{\varepsilon - 1}{\varepsilon + 2} - \frac{n^2 - 1}{n^2 + 2}\right]$$

$$m_2 = \frac{2}{hca^3}(\mu_e - \mu_g)^2$$

Ravi's equation (described in main text):[5]

$$\nu_a - \nu_f = m_3 E_T^N + constant$$

$$m_3 = 11307.6\left[\left(\frac{\delta\mu}{\delta\mu_B}\right)^2\left(\frac{a_B}{a}\right)^3\right]$$

$$\Leftrightarrow \mu_e - \mu_g = \sqrt{\frac{m_3 \times 81}{(6.2/a)^3 11307.6}}$$

In Ravi's equation, $\delta\mu_B$ and a_B are the dipole moment change upon excitation and the Onsarger radius of a betaine dye, respectively.

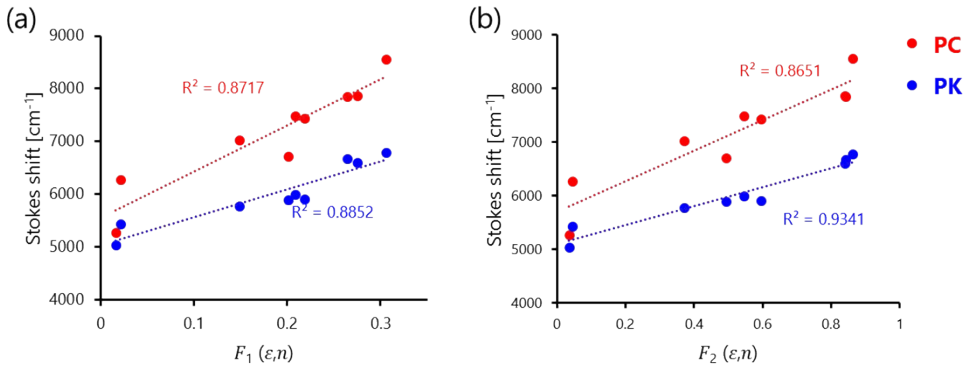

Figure S2. The variation in the Stokes shifts of **PC** (red) and **PK** (blue) with solvent function: $F_1(\varepsilon,n)$ (Lippert–Mataga equation) and $F_2(\varepsilon,n)$ (Bakhshiev's equation).

Table S1. The change in the dipole moment between the ground and excited states of **PC** and **PK**.

	a [Å]	m_1	m_2	m_3	$\delta\mu$ (Lippert–Mataga) [Debye][a]	$\delta\mu$ (Bakhshiev) [Debye]	$\delta\mu$ (Ravi) [Debye]
PC	4.62	8,750	2,855	5,337	9.27	5.30	3.94
PK	4.38	5,289	1,780	3,199	6.65	3.86	3.18

[a]1 Debye = 3.33564×10^{-30} cm = 10^{-18} esu cm.

4. Optimized structures and dipole moments of PC and PK in the ground and excited states

The theoretical dipole moments of **PC** and **PK** in the ground and excited states were obtained from their optimized structures in each state, which were estimated from DFT and time-dependent DFT (TDDFT) calculations, respectively, using the Gaussian 09 program package.[2] To reduce calculation burden, the piperidinyl groups of both **PC** and **PK** were replaced by *N,N*-dimethylamino groups. Similarly, the alkyl chain ($-C_3H_7$) of the vinyl ketone structure of **PC** was replaced with a $-CH_3$ moiety. All calculations were performed assuming vacuum conditions.

First, the equilibrium structures of **PC** and **PK** in the ground state were fully optimized using the M062X method with the 6-31+G** basis set. The analytical frequencies were obtained to ensure that a local energy minimum was located. Next, the Frank–Condon states of **PC** and **PK** in the excited states were estimated by TDDFT calculations. Finally, the equilibrium structures of **PC** and **PK** in the excited states were fully optimized using the M062X method with the 6-31+G** basis set.

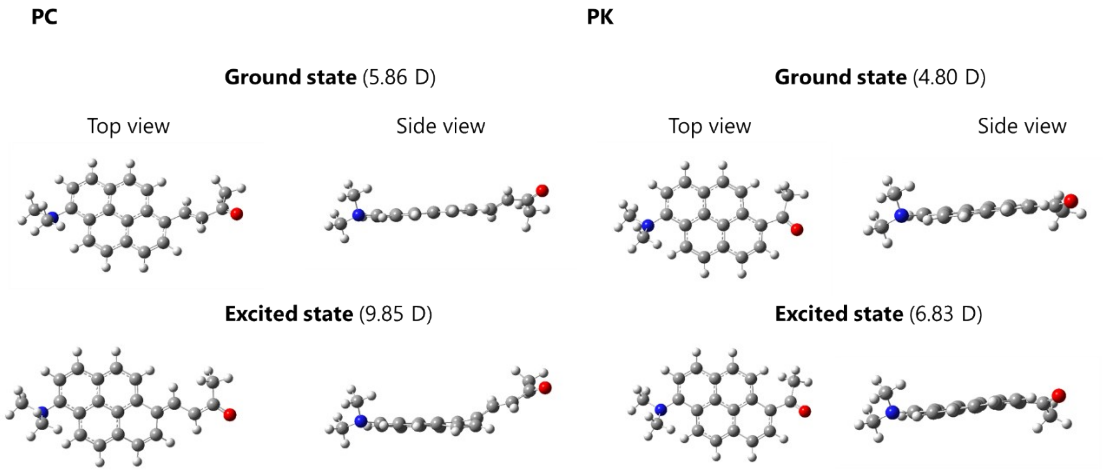

Figure S3. Optimized structures and dipole moments of **PC** and **PK** in the ground and excited states.

5. Time-resolved fluorescence decay of PC and PK in large unilamellar vesicles (LUVs) of different lipid compositions

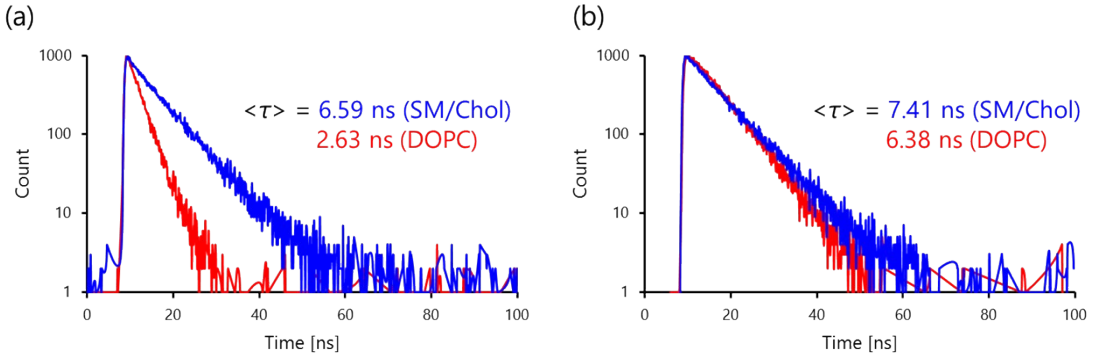

Figure S4. Fluorescence decay profiles of (a) **PC** and (b) **PK** in large unilamellar vesicles (LUVs) of different composition. Dye concentration: 1 µM; lipid concentration: 200 µM (phosphate buffer 20 mM, pH 7.2); excitation wavelength: 405 nm. Fluorescence was monitored at the fluorescence maximum wavelength of the dyes in each LUV, as described in Table 1 in the manuscript. Definitions: DOPC = 1,2-dioleoyl-sn-glycero-3-phosphocholine; SM/Chol = sphingomyelin/cholesterol.

6. Confocal laser scanning fluorescence microscopy (CLSM) images of PC3 cells stained by PC and Lipi-Deep Red.

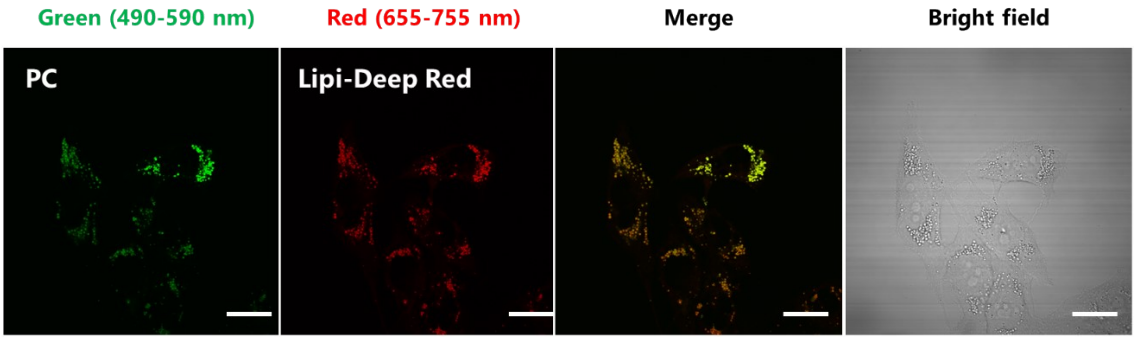

Figure S5. Confocal laser scanning fluorescence microscopy (CLSM) fluorescence images of PC3 cells. The fluorescence of **PC** was detected with a green channel under 405 nm of excitation light. Similarly, the fluorescence of Lipi-Deep Red was detected with a red channel under 635 nm of excitation light. Probe concentration: 0.5 μM; scale bars: 20 μm.

7. Cytotoxicities of PC and PK

The cytotoxicities of **PC** and **PK** were estimated by MTT assay. First, the human keratinocyte K16 cells were seeded in collagen-coated 96-well dishes (11,500 cells /well). **PC-** or **PK**-containing new medium was added after 4 d from cell seeding. After 24 h, the **PC-** or **PK**-containing medium was exchanged and 10 μL of thiazolyl blue tetrazolium bromide solution (5 mg/mL in HBSS buffer solution, Sigma–Aldrich, St. Louis, MO, USA) was added to each well. The cells were killed by adding 100 μL of a 10% SDS solution after incubating for 3 h at 37 °C. The absorbance at 570 nm was measured using a Spectra Max 180 microplate reader (Molecular Devices, San Jose, CA, USA) after incubating overnight at 37 °C.

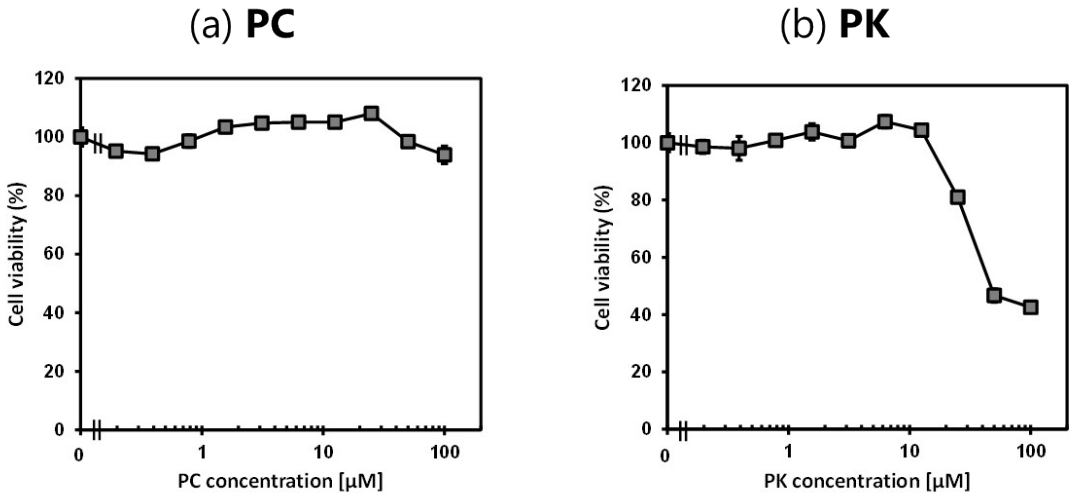

Figure S6. Cell viabilities after incubation with (a) **PC** and (b) **PK** for 24 h.

8. Comparison of PC, PK, and Nile Red (NR) in human tissue imaging using two-photon fluorescence microscopy (2PM)

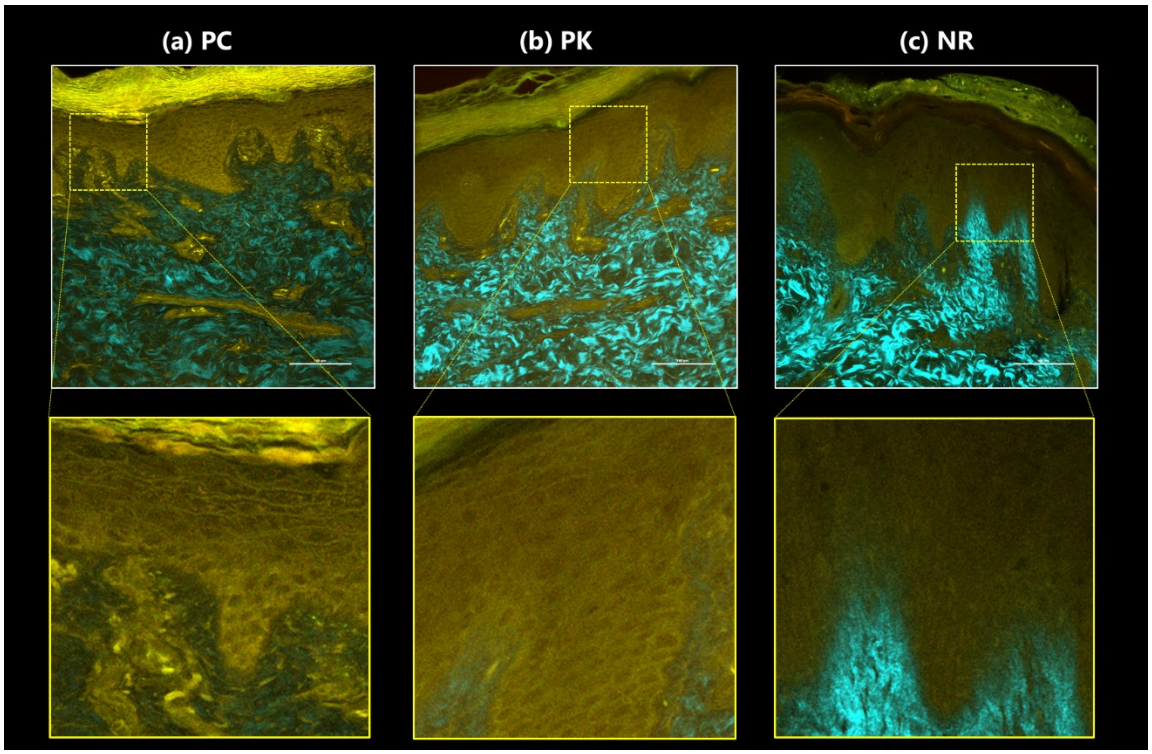

Figure S7. Two-photon fluorescence microscopy (2PM) images of normal human tissue blocks stained with (a) **PC**, (b) **PK**, and (c) Nile Red (**NR**). All tissues were treated with LUCID to enhance their transparencies during the probe staining process. Probe concentration: 10 μM; excitation wavelength: 960 nm; cyan channel: 492 nm; green channel: 500–550 nm; orange channel: 560–593 nm; red channel: 593 nm.

9. ^{1}H and ^{13}C NMR spectra of PC and PC2.

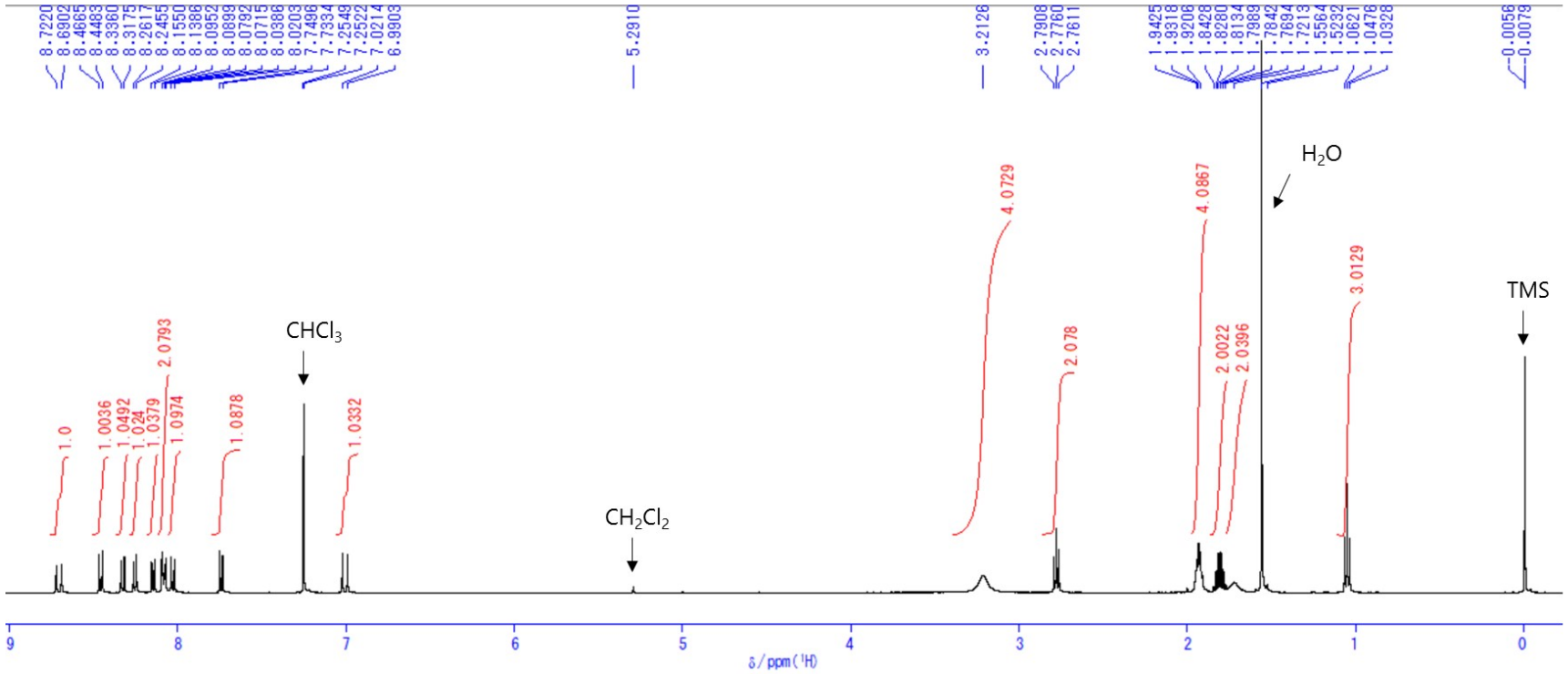

Figure S8. ^{1}H NMR spectrum of **PC** (500 MHz, $CDCl_3$).

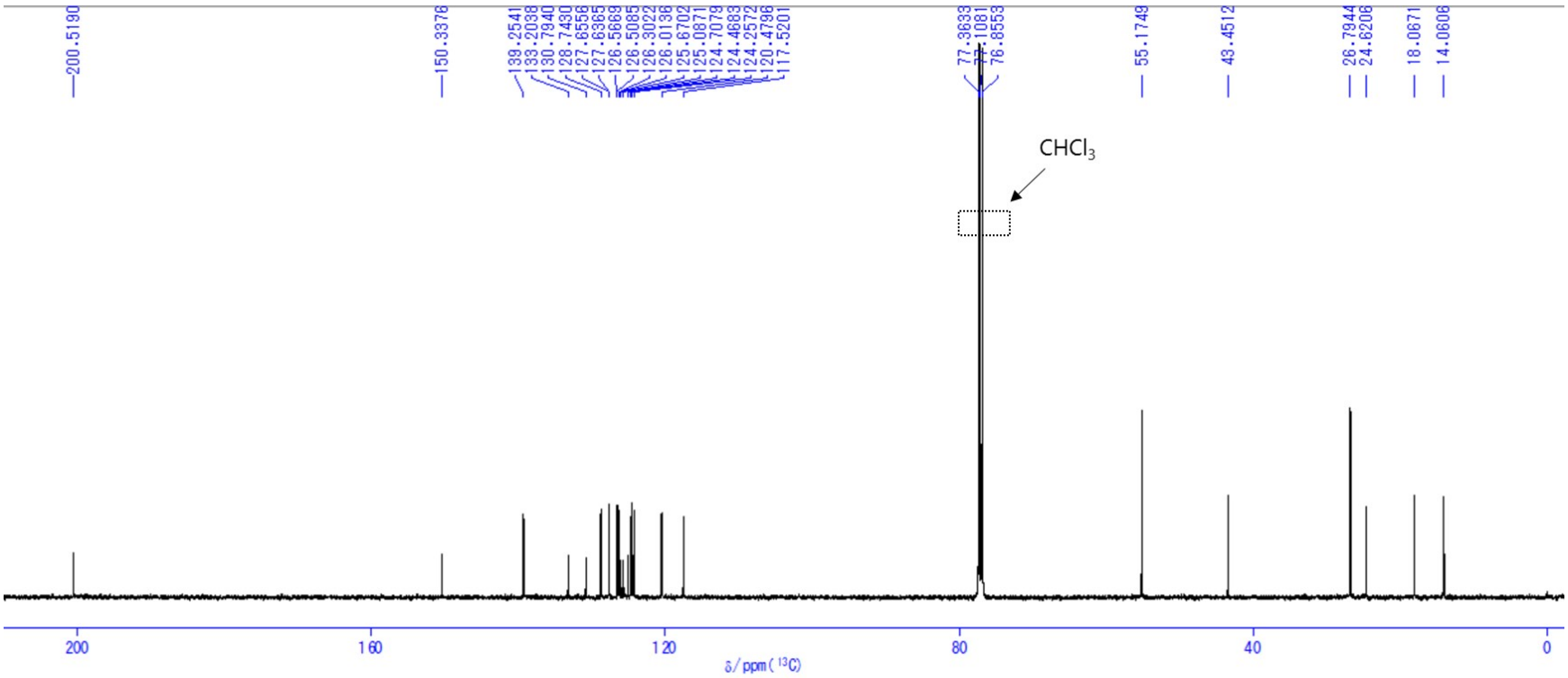

Figure S9. ^{13}C NMR spectrum of **PC** (125 MHz, $CDCl_3$).

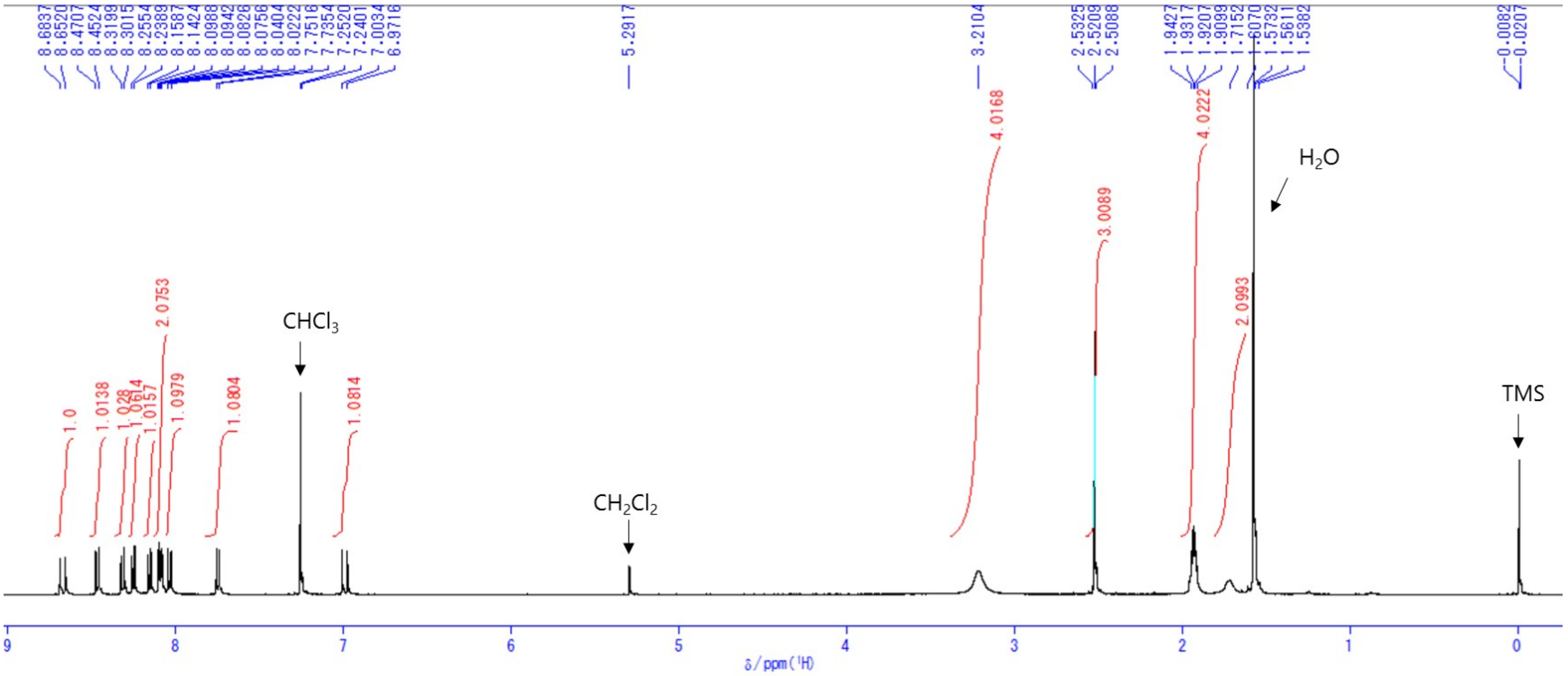

Figure S10. ^{1}H NMR spectrum of **PC2** (500 MHz, $CDCl_3$).

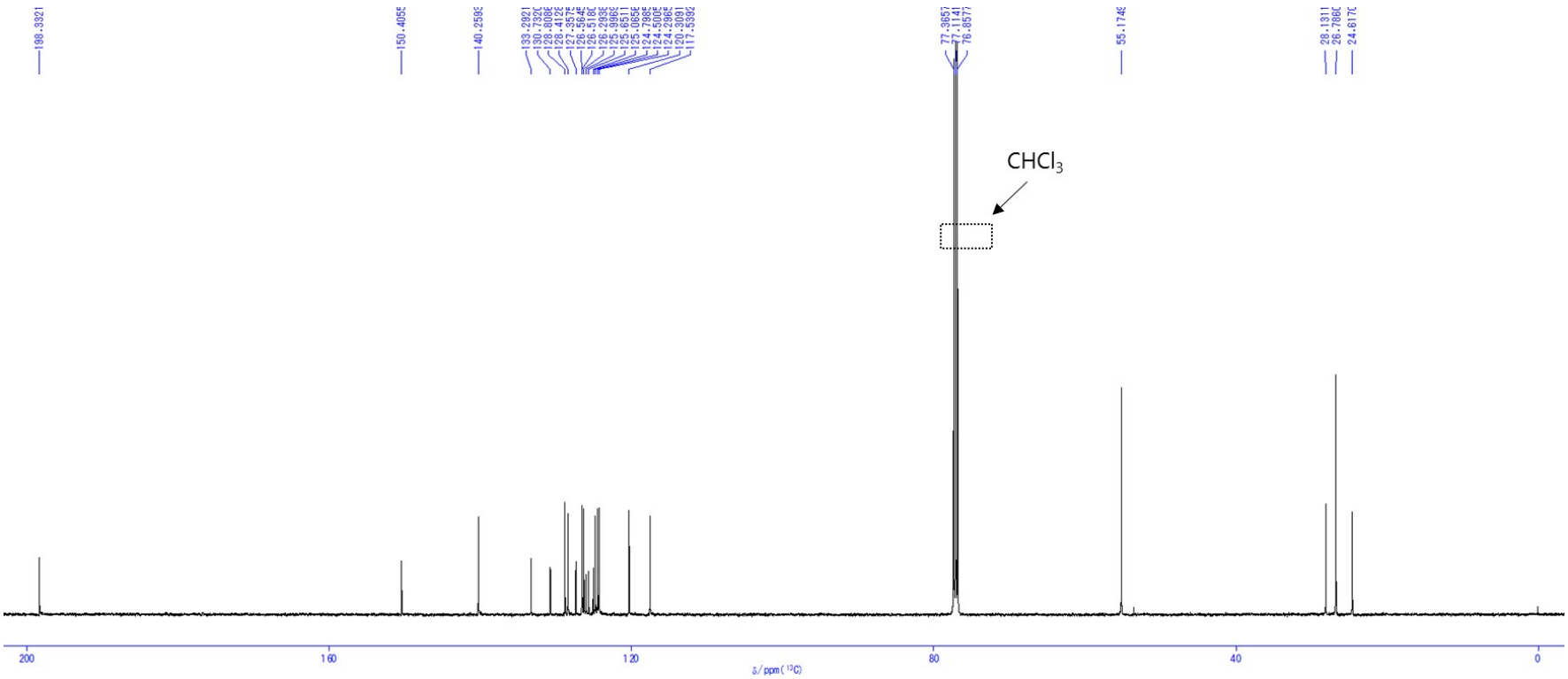

Figure S11 ^{13}C NMR spectrum of **PC2** (125 MHz, $CDCl_3$).

References

1. Y. Niko, S. Kawauchi and G. I. Konishi, *Chem. Eur. J.*, 2013, **19**, 9760–9765.
2. M. J. Frisch, G. W. Trucks, H. B. Schlegel, G. E. Scuseria, M. A. Robb, J. R. Cheeseman, G. Scalmani, V. Barone, B. Mennucci, G. A. Petersson, H. Nakatsuji, M. Caricato, X. Li, H. P. Hratchian, A. F. Izmaylov, J. Bloino, G. Zheng, J. L. Sonnenberg, M. Hada, M. Ehara, K. Toyota, R. Fukuda, J. Hasegawa, M. Ishida, T. Nakajima, Y. Honda, O. Kitao, H. Nakai, T. Vreven, J. A. Montgomery Jr, J. E. Peralta, F. Ogliaro, M. Bearpark, J. J. Heyd, E. Brothers, K. N. Kudin, V. N. Staroverov, R. Kobayashi, J. Normand, K. Raghavachari, A. Rendell, J. C. Burant, S. S. Iyengar, J. Tomasi, M. Cossi, N. Rega, J. M. Millam, M. Klene, J. E. Knox, J. B. Cross, V. Bakken, C. Adamo, J. Jaramillo, R. Gomperts, R. E. Stratmann, O. Yazyev, A. J. Austin, R. Cammi, C. Pomelli, J. W. Ochterski, R. L. Martin, K. Morokuma, V. G. Zakrzewski, G. A. Voth, P. Salvador, J. J. Dannenberg, S. Dapprich, A. D. Daniels, Ö. Farkas, J. B. Foresman, J. V. Ortiz, J. Cioslowski and D. J. Fox, Gaussian, Inc., Wallingford CT, Gaussian, 2013, **09**, Revision D.01.
3. E. Lippert, *Z. Elektrochem.*, 1975, **61**, 962–975.
4. N. G. Bakhshiev, *Opt. Spectrosc.*, 1964, **16**, 821–825.
5. M. Ravi, T. Soujanya, A. Samanta and T. P. Radhakrishnan, *Faraday Trans.*, 1995, **91**, 2739–2742.